Coupled mode analysis of micro-disk resonators with an asymmetric- index-profile coupling region

Clément Arlotti, Guilhem Almuneau, Olivier Gauthier-Lafaye, Stéphane Calvez

Coupled mode analysis of micro-disk resonators with an asymmetric-index-profile coupling region

C. Arlotti*[a], G. Almuneau [a], O. Gauthier-Lafaye [a] S. Calvez [a]
[a] CNRS, LAAS, 7 avenue du colonel Roche, F-31400 Toulouse, France
Univ. de Toulouse, UPS, LAAS, F-31400 Toulouse, France

ABSTRACT

In this article, we apply the coupled-mode theory to vertically-coupled micro-disk resonators presenting an asymmetric distribution of refractive index and a multilayer separation region between the two waveguide cores, resulting in an effective propagation constant phase-mismatch in the coupling region. We introduce a criterion which, given the coupler overall permittivity distribution, clarifies how to best choose the individual decomposition index profiles among the various possible solutions. Following our recent experimental demonstration we subsequently exploit the derived decomposition to evaluate the theoretical transmission characteristics of an AlGaAs/AlOx-based structure as function of wavelength and as function of the position of the resonator relative to the access waveguide.We show that the resonant dips of the intensity transmission, spaced by the cavity FSR, are modulated by an envelop which governs the coupling regime of the resonator-waveguide system.

Keywords: resonator, disk, whispering gallery mode, coupled modes theory, vertical coupling

1. INTRODUCTION

Over the last two decades, integrated whispering-gallery-mode resonators have been increasingly used as the basic building blocks for selective filters, high-sensitivity sensors, nonlinear converters, or even as low-threshold lasers[1–3]. Irrespective of the application, the performance of these integrated micro-resonators is generally governed by the evanescent coupling of the light between its constitutive cavity and access waveguides, and their usefulness relies on the ability to obtain high-quality factors. To do so, it is necessary to achieve the critical coupling condition where the system transfer function drops to zero due to destructive interference between the input waveguide incident field and the outcoupled resonator field[4]. It is therefore of crucial importance to be able to assess the dependence of the coupler characteristics based on the chosen structural layout. The coupled-mode theory, which derives the response of a full coupler from the linear superposition of a number of constitutive decomposition fields, has been shown to be one of the most efficient methods to describe this coupling interaction for devices with simple and often symmetric refractive index distributions[5–7].

Here, following our recent experimental demonstration, we extend the coupled-mode analysis to vertically-coupled micro-disk resonators presenting not only an asymmetric distribution of refractive index but also a multilayer separation region between the two waveguide cores, generally resulting in mismatched propagation constants in the coupling region. In doing so, we introduce a criterion which, given the coupler overall permittivity distribution, clarifies how to best choose the individual decomposition index profiles among the various possible solutions. We subsequently exploit the derived decomposition to evaluate the theoretical transmission characteristics of an AlGaAs/AlOx-based structure as function of wavelength and as function of the position of the resonator relative to the access waveguide. We show that the resonant dips of the intensity transmission, spaced by the cavity FSR, are modulated by an envelop that governs the coupling regime of the resonator-waveguide system. The control of this envelop's shape relies on the coupler characteristics and offers various possibilities in the design of critically-coupled devices.

published in *proc. of SPIE* Volume 10090 – article 10090-48

2. INTRODUCTION TO COUPLED MODES THEORY

The coupled-mode theory (CMT) assumes that the total field $(\widetilde{\boldsymbol{E}}(x,y,z), \widetilde{\boldsymbol{H}}(x,y,z))$for the complete structure can be linearly decomposed over the eigen-mode basis of each constituting waveguide of the structure[5, 8]. Each of the eigen-modes $\widetilde{\mathbf{E}}_m(x,y,z)$ of these waveguides (consisting of the lateral mode profiles $\mathbf{E}_m(x,y)$multiplied by the appropriate z exponential dependence) is modulated by an amplitude function $A_m(z)$ that evolves with the propagation coordinate z.

$$\begin{cases} \widetilde{\boldsymbol{E}}(x,y,z) = \sum_m A_m(z)\widetilde{\boldsymbol{E}}_m(x,y,z) \\ \widetilde{\boldsymbol{H}}(x,y,z) = \sum_m A_m(z)\widetilde{\boldsymbol{H}}_m(x,y,z) \end{cases} \quad (1)$$

$$\text{Where } \begin{cases} \widetilde{\boldsymbol{E}}_m(x,y,z) = \boldsymbol{E}_m(x,y)e^{-i\beta_m z} \\ \widetilde{\boldsymbol{H}}_m(x,y,z) = \boldsymbol{H}_m(x,y)e^{-i\beta_m z} \end{cases} \quad (2)$$

There are several ways to establish the evolution equation for the amplitudes $A_m(z)$ among which figure the variational method[9] or the Lorentz reciprocity theorem[5,8,9]. The underlying principle is that, once power-normalized, the overall field decomposition (1) is adequately combined with one of the basis electromagnetic field $\mathbf{E}_k(x,y,z), \mathbf{H}_k(x,y,z)$ and integrated over the whole transverse section to obtain the evolution equation for the amplitudes $\mathrm{A}_m(z)$:

$$\sum_m \frac{dA_m}{dz} \iint \boldsymbol{e}_z . \left(\widetilde{\boldsymbol{E}}_m \times \widetilde{\boldsymbol{H}}_k^* + \widetilde{\boldsymbol{E}}_k^* \times \widetilde{\boldsymbol{H}}_m\right) dxdy = -i\omega\varepsilon_0 \sum_m A_m \iint (\varepsilon - \varepsilon_m)\, \widetilde{\boldsymbol{E}}_m \cdot \widetilde{\boldsymbol{E}}_k^* dxdy \quad (3)$$

Where $4P_m = \iint \boldsymbol{e}_z . (\boldsymbol{E}_m \times \boldsymbol{H}_m^* + \boldsymbol{E}_m^* \times \boldsymbol{H}_m) dxdy = 1$ represents the normalized optical power carried by eigen-mode m.

$\kappa_{km} = \omega\varepsilon_0 \iint (\varepsilon - \varepsilon_m)\, \boldsymbol{E}_m \cdot \boldsymbol{E}_k^* dxdy$ represent the first-order evanescent coupling coefficients from waveguide m to waveguide k. This parameter quantifies how efficiently the power transfers between the two parallel waveguides

$c_{km} = \iint \boldsymbol{e}_z . (\boldsymbol{E}_m \times \boldsymbol{H}_k^* + \boldsymbol{E}_k^* \times \boldsymbol{H}_m) dxdy$ is the butt-coupling coefficient or cross-power matrix-element. It represents the excitation efficiency from a field propagating into a waveguide with an eigen-modes basis $\{\boldsymbol{E}_m(x,y)\}$ to a field propagating into a waveguide with an eigen-modes basis $\{\boldsymbol{E}_k(x,y)\}$.

$\kappa_{mm} = \omega\varepsilon_0 \iint (\varepsilon - \varepsilon_m)\, \boldsymbol{E}_m \cdot \boldsymbol{E}_m^* dxdy$ represent the second-order evanescent coupling coefficients or self-coupling of waveguide (or mode) m to itself.

3. COUPLER PERMITTIVITY DECOMPOSITION

Given the coupler overall permittivity distribution, one has to define the individual decomposition index profiles in order to build the total field solution (1).

Picking one decomposition over another is not necessarily straightforward, especially for couplers with a multilayer asymmetric permittivity profile. Moreover the reasons for this choice are often eluded in the relevant litterature[5,8,10]. It is however important to carefully consider the choice of these individual index profiles, as it results in the definition of the constitutive waveguides that support the eigen-mode basis used to build the aforementioned linear decomposition of the total optical field in the full coupler structure. In the derivation of the first order evanescent coupling coefficient κ_{km}, the difference $\Delta\varepsilon_m = \varepsilon - \varepsilon_m$ between the coupler overall permittivity distribution ε and the individual permittivity decomposition ε_m represents a refractive index perturbation to guide m. This perturbation is induced by the presence of a reference waveguide k that exchanges power from waveguide m with a guided mode of waveguide k. Hence, the meaning of $\kappa_{km} = \omega\varepsilon_0 \iint (\varepsilon - \varepsilon_m)\, \boldsymbol{E}_m \cdot \boldsymbol{E}_k^* dxdy$: the power transfer from guiding element m to guiding element k.

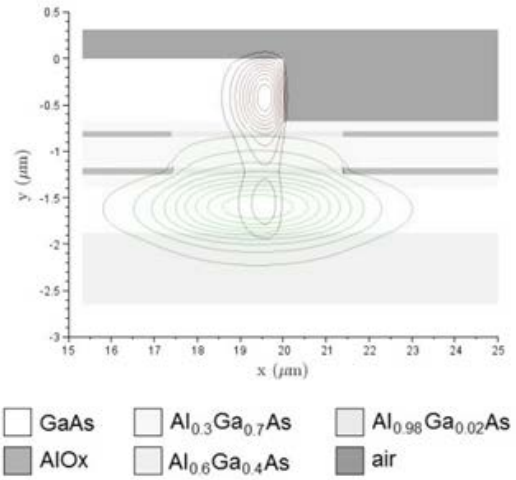

Figure 1. Cross section diagram of the waveguide-resonator coupling region

The structure under investigation is the one we recently demonstrated[11] and its vertical index profile in the coupling region is depicted in figure 1.
Our criterion to select the permittivity decomposition applies to coupler structures with piece-wise constant overall permittivity distributions ε, as represented in figure 2.
It consists in picking individual permittivity distributions ε_m such that, on each piece of the distribution, the value of the difference $\Delta\varepsilon_m = \varepsilon - \varepsilon_m$ is either zero or positive and as small as possible, in order to best fit the perturbative nature of the CMT. Moreover, we choose ε_m such that the permittivity perturbation value $\Delta\varepsilon_m$ is minimized, positive and non-zero only in the region of the core of waveguide k, and zero everywhere else.
This choice restricts the integration domain to the latter region and allows better understanding of the meaning of κ_{km}, that is, the evanescent field overlap leading to a guided power transfer from waveguide m to the core of waveguide k.
The constitutive waveguides defined that way best reproduce the total structure of the coupler and, as a matter of fact, lead to more accurate linear decompositions of the total field.

Due to the simplicity of deriving their eigen-modes, 3-layer slab-like individual permittivity decompositions ε_m are often proposed as equally efficient alternatives to multilayer (more than 3 layers) decompositions in the relevant litterature[5,8,10]. They however have an important drawback when it comes to decomposing copulers with asymmetric multilayer permittivity distributions ε. Indeed, in this case, the $\Delta\varepsilon_m$ values are no longer piece-wise minimized as they can become positive (resp. negative) in regions outside of the core of waveguide k, as shown in figure 2. This is considered as an artefact in the integration domain of the mode overlap coupling coefficients that unduly increases (resp. lowers) their value. Moreover, as the wavelength increases the effective indices of these individual 3-layer waveguides increasingly differ from those of the supermodes of the complete structure supported by ε.
Our permittivity decomposition choice criterion permits to avoid the drawbacks of the latter artefact at the price of a "multilayer" decomposition, whose eigen-modes are slightly more complex to derive, but is better-suited as more perturbative.

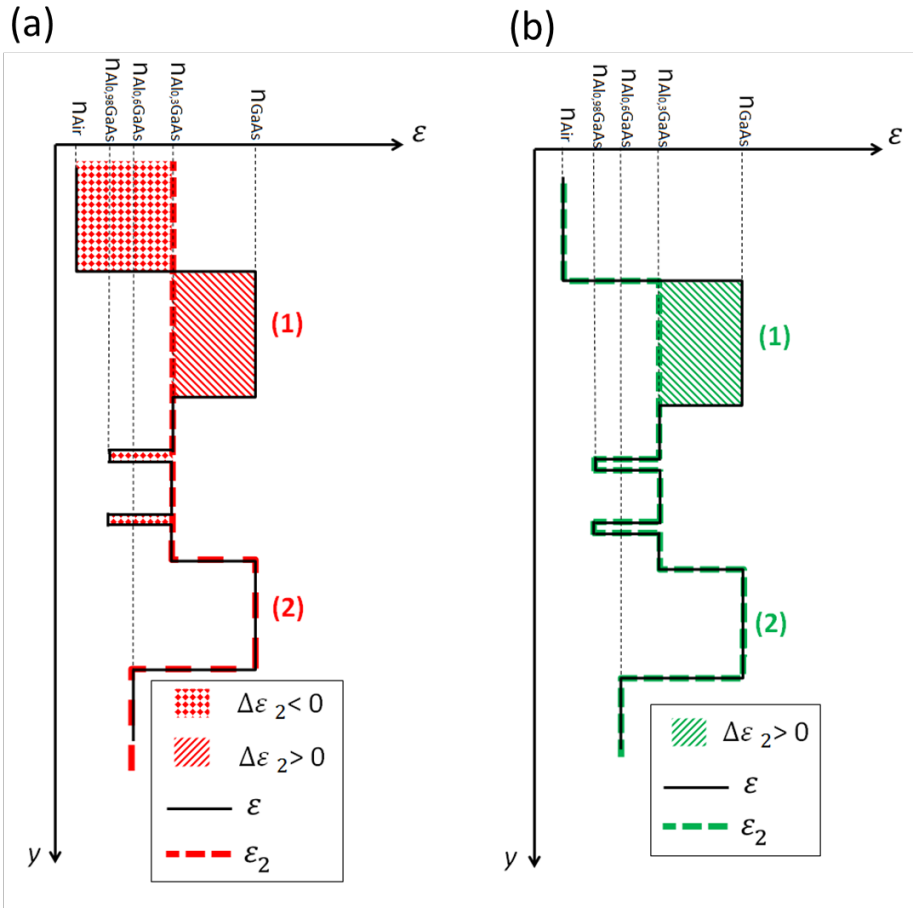

Figure 2. Representation of the resonator-waveguide (resp. (1) and (2)) permittivity distribution in the coupling region. (a) commonly-used 3-layer individual permittivity decomposition of waveguide (2) leading to negative-perturbation zones. (b) multi-layer permittivity decomposition of waveguide (2), following our aforementioned criterion.

Figure 3 displays the reduced form of the mode overlap coupling coefficients yielded by the individual permittivity decompositions described in fig. 2. It highlights the importance of the permittivity decomposition criterion. Indeed, Panel (a) demonstrates that the 3-layer decomposition is in fact inadequate for the following two reasons: first, the coefficient κ_a changes sign at a wavelength close to 1250 nm, whilst κ_b remains positive. and the the values of the second-order self-coupling coefficients $\alpha_{a,b}$ are greater than the first order mutual-coupling coefficients $\kappa_{a,b}$, which is incoherent with standard CMT predictions. Panel (b) also shows that multi-layer permittivity decompositions described in fig. 2.b, which follows our selection criterion, does not exhibit the above-mentioned pitfalls.

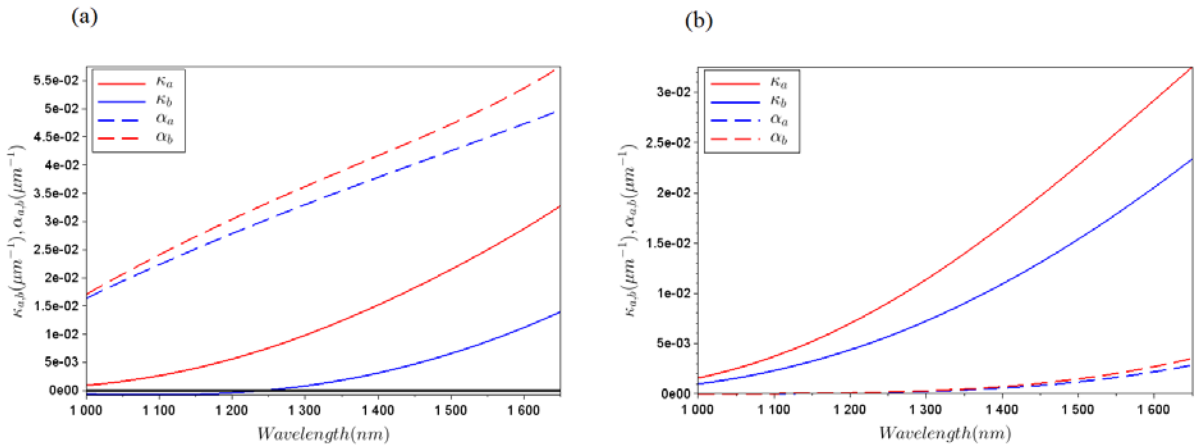

Figure 3. Evolution of the reduced form of the mode overlap coupling coefficients as function of wavelength yielded by (a) commonly-used 3-layer individual permittivity decompositions as described in fig. 2.a. (b) multi-layer permittivity decompositions as described in fig. 2.b.

4. COUPLED-MODE MODEL OF THE STRUCTURE

It has been shown that monomode vertical coupling between a WGM resonator and its access waveguide can be accurately modeled as coupling between two parallel slab waveguides using standard CMT[6,7]. In this approximation, the interaction length L of the defined 1-D slab-like coupler is set up by the length of the overlap between the waveguide and the resonator and can be adjusted by changing their lateral alignment X_0 as shown in figure 4. This approximation holds as long as the position of the center of the access waveguide is above the radius R_c of the internal caustic of the disk mode. The coupling length L has a geometrical dependence on the disk radius R, the access-waveguide width W and the lateral offset x_0 : $L = 2\sqrt{(W - x_0)(2R + x_0 - W)}$

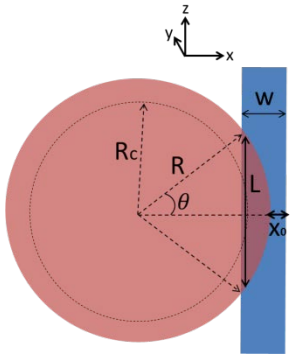

Figure 4. Top view schematic of the waveguide-resonator overlap in the coupling region. Changing the lateral offset $x_0$permits to adjust the coupling interaction length L.

Applying the evolution equation (3) to the case of a vertically monomode access waveguide and resonator (i.e. 2 modes in the entire structure) results in a coupled system of two first-order differential equations :

$$\begin{cases} \frac{dA_1}{dz} = -i\kappa_a A_2 e^{-i2\delta z} + i\alpha_a A_1 \\ \frac{dA_2}{dz} = -i\kappa_b A_1 e^{i2\delta z} + i\alpha_b A_2 \end{cases} \qquad (4)$$

Where $\delta = \frac{\beta_2 - \beta_1}{2}$ is the propagation constant mismatch and $\kappa_a = \frac{\kappa_{12} - c_{12}\kappa_{22}}{1-|c_{12}|^2}$, $\kappa_b = \frac{\kappa_{21} - c_{12}^* \kappa_{11}}{1-|c_{12}|^2}$, $\alpha_a = \frac{\kappa_{12} c_{12} - \kappa_{11}}{1-|c_{12}|^2}$, $\alpha_b = \frac{\kappa_{12} c_{12}^* - \kappa_{22}}{1-|c_{12}|^2}$ are the reduced form of the mode-overlap coupling coefficients[12.]

After some algebra, the amplitudes of the optical fields at the input/output ports of the coupler are related by the CMT coupling matrix[12] :

$$\begin{pmatrix} A_1(L) \\ A_2(L) \end{pmatrix} = M_{CMT} \begin{pmatrix} A_1(0) \\ A_2(0) \end{pmatrix} \qquad (5)$$

$$M_{CMT} = \begin{pmatrix} [\cos(\Gamma L) + j\frac{\hat{\delta}}{\Gamma}\sin(\Gamma L)]e^{-j(\hat{\delta}-\alpha_a)L} & -j\frac{k_a}{\Gamma}\sin(\Gamma L)e^{-j(\hat{\delta}-\alpha_a)L} \\ -j\frac{k_b}{\Gamma}\sin(\Gamma L)e^{j(\hat{\delta}+\alpha_b)L} & [\cos(\Gamma L) - j\frac{\hat{\delta}}{\Gamma}\sin(\Gamma L)]e^{j(\hat{\delta}+\alpha_b)L} \end{pmatrix} \qquad (6)$$

Where $\hat{\delta} = \delta + \frac{\alpha_a - \alpha_b}{2}$ and $\Gamma = \sqrt{\kappa_a \kappa_b + \hat{\delta}^2}$

Butt-coupling and self-coupling coefficients are usually neglected in standard analysis[6], when the propagation constants of the two waveguides are matched $(\delta = 0)$ or very similar $(\delta \approx 0)$ or when the two waveguides are operating in the weak coupling regime (i.e. are sufficiently separated from each other $(c_{12} \cong 0)$[12]). However, when two waveguides with mismatched propagation constants are placed close together (strong coupling regime), c_{km} and κ_{mm} must be taken into account. Moreover, when the coupling interaction is not adiabatically set up, butt-coupling coefficient cannot be neglected either. That is typically the case of vertical coupling, where the two waveguides "see" an abrupt transverse refractive index perturbation build-up along the propagation axis, when entering the transition zone of the coupling region.

The feedback established by the propagation along the whispering-gallery-mode resonator with intrinsic loss rate $\frac{\rho}{2}$ imposes the following relationship between the resonator amplitude fields $A_2(0)$ and $A_2(L)$:

$$A_2(0) = A_2(L)e^{-i\beta_R(L_R - L) - \frac{\rho}{2}L_R} = A_2(L)e^{i\theta}\alpha \qquad (7)$$

Where $\alpha = e^{-\frac{\rho}{2}L_R}$,the inner cicrulation factor, represents the internal losses.

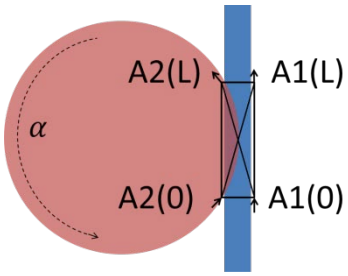

Figure 5. Sketch of the two-port codirectional coupler model

Plugging this condition into the system of equations (5)-(6) yields an expression of the transmitted intensity of the optical field through the waveguide after coupling to the resonator :

$$T(\varphi) = \left|\frac{A_1(z)}{A_1(0)}\right|^2 = \frac{|t|^2+\alpha^2-2\alpha|t|\cos(\beta_R(L_R-L)+\phi_t)}{1+|t|^2\alpha^2-2\alpha|t|\cos(\beta_R(L_R-L)+\phi_t)} \quad (8)$$

Where $t = \cos(\Gamma L) + j\frac{\hat{\delta}}{\Gamma}\sin(\Gamma L) = |t|e^{-i\varphi_t}$ is the transmission coefficient of the codirectional coupler and $\varphi = \beta_R(L_R - L) + \phi_t$ is the total phase-shift over one round trip in the resonator, with $\phi_t = \varphi_t - (\hat{\delta} + \alpha_b)L + \beta_R L$ being the complete-CMT phase-shift introduced by the coupler.

At resonance, the transfer function T reaches its minimum and

$$\varphi = \beta_R(L_R - L) + \phi_t = 2m\pi \quad (9)$$

Equation (8) can be rewritten in the form of a Lorentzian dip by performing a series expansion in the vicinity of a resonance φ_0 when the total phase shift $\varphi = 2m\pi$ ($m \in \boldsymbol{Z}$), which leads to the expression of the Q factor of the cavity :

$$Q = \frac{\sqrt{\alpha|t|}(\beta_R(L_R-L)+\phi_t)}{2(1-\alpha|t|)} \quad (10)$$

The resonance condition (8) defines a set of dips and peaks spectrally separated by the cavity FSR and modulated by an envelop whose expressions is :

$$T_{res-} = \frac{|t|^2+\alpha^2-2\alpha|t|}{1+|t|^2\alpha^2-2\alpha|t|} = \frac{(\alpha-|t|)^2}{(1-\alpha|t|)^2} \quad (11)$$

The critical coupling condition is achieved when the internal losses α in the resonator are equal to the coupling losses $|t|$. Then the transmitted power (11) drops to zero due to perfect destructive interference in the outgoing waveguide between the non-coupled transmitted field and the internal cavity field coupled to the output waveguide[4] as will be shown in figure 7.

5. COUPLED-MODE ANALYSIS OF THE STRUCTURE

In this section, we investigate the coupled microdisk characteristics of the recently-reported and above-described vertically-coupled structure[11]. The microdisk diameter is taken to be 300 µm and the coupler length is varied to simulate various guide-to-resonator offsets.

The reduced form of the mode overlap coupling coeffcients $\kappa_{a,b}$and $\alpha_{a,b,}$ shown in figure 3, supported by the complete set of mode overlap coupling coefficients $\kappa_{12}, \kappa_{21}, c_{12}, \kappa_{11}, \kappa_{22}$, were evaluated by numerical integration of the eigen-mode profiles overlap along the vertical axis. The mode profiles and effective indices were obtained (with a homemade script) by solving an interface problem given the constitutive permittivity decompositions and the continuity conditions for the tangential components of the electromagnetic field.
The resonator loss were assumed to be soly due to surface scattering due to roughness imperfections of the cavity walls, since the bending losses are negligible for large radii WGMs. The surface scattering quality factor Q_{ss} for TE modes of the disk can be approximed by the Volume Current Method which yields an analytic expression[13] that depends on the effective indices, as well as geometrical and roughness parameters. We implemented it with a rms roughness $\sigma_r = 3$ nm and a roughness coherence length of $l_{cr} = 100$ nm in order to compute the scattering loss rate $\rho_{scatter} = \frac{2\pi n_{eff}}{\lambda Q_{ss}}$ (cm^{-1}) shown in figure 6.

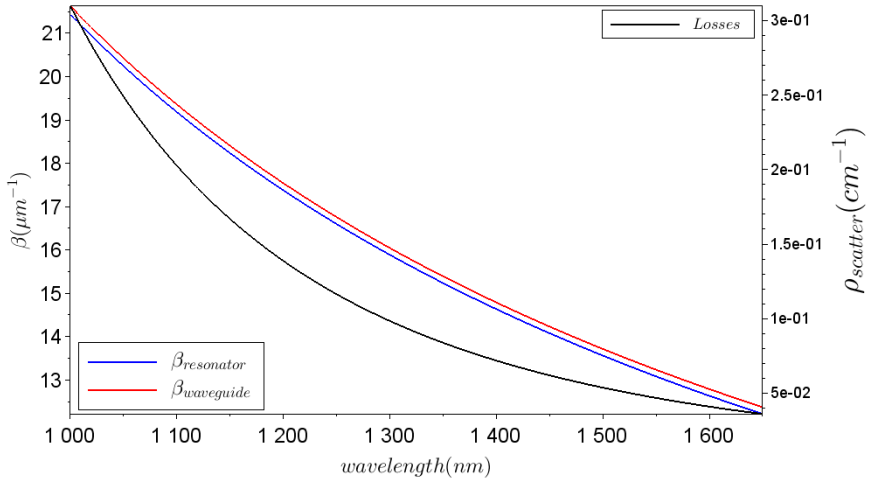

Figure 6. Evolution of the disk resonator and access waveguide effective propagation constants (resp. blue and red curve) and resonator scattering losses (black curve) with wavelength

We subsequently exploit the derived mode-overlap coefficients and loss rate as basic building blocks of the transfer function (11) to evaluate the theoretical transmission characteristics of the coupled resonator as function of wavelength and as function of the coupling length L.

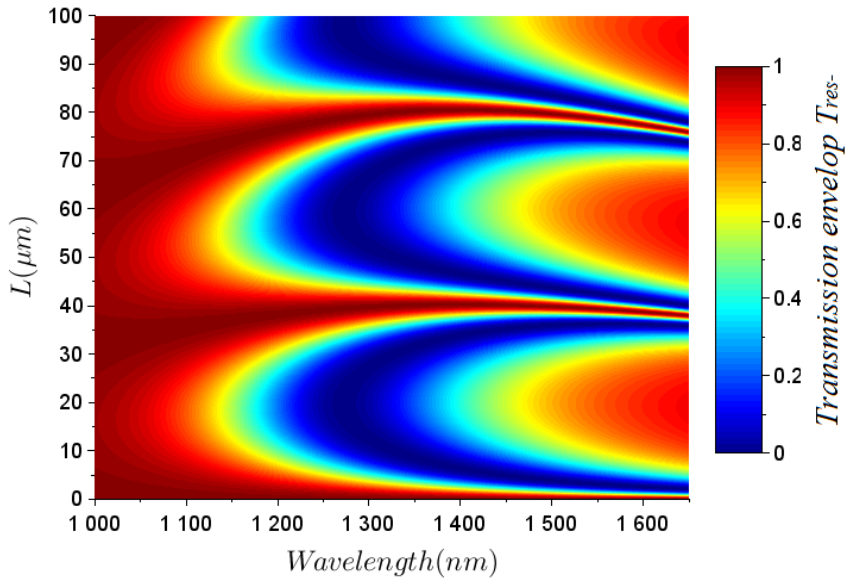

Figure 7. Transmission envelop T_{res-} of the vertically coupled structure as a function of wavelength and coupling length

As shown in figure 7, the cross-section of the transmission T_{res-} at $\lambda = 1550\ nm$ displays a number of coupling length values where critical coupling occurs, i.e. $T_{res-} = 0$ and $Q = Q_c = \frac{Q_{int}}{2}$, with $Q_{int} = \frac{\sqrt{\alpha}(\beta_R(L_R - L) + \phi_t)}{2(1-\alpha)}$ the intrinsic quality factor corresponding to an uncoupled resonator (i.e. $|t| = 1$). Each of these critical coupling lengths yields different transmission shapes and bandwidths.

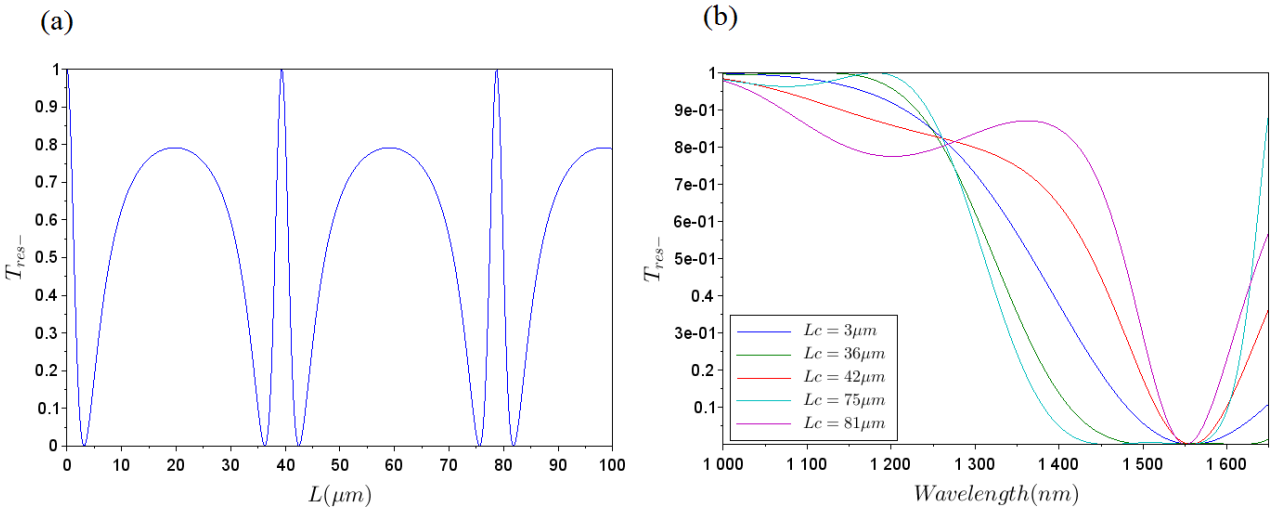

Figure 8. (a) Cross-section of the transmission T_{res-} at $\lambda = 1550$ nm. (b) Representation T_{res-} as a function of wavelength for each of the critical coupling lengths of panel (a)

For instance, panel (b) of figure 8 shows a narrow band transmission corresponding to Lc = 81µm, whereas panel (a) shows a broadband transmission for Lc = 36 µm. The broadest transmission bands correspond to the largest $Q \approx Q_c$ zones.

Figure 9 shows that the Q-factor goes from under ($Q > Q_c$) to over-coupling ($Q < Q_c$) regime. This because of the periodic exchange of power in the coupler. This typically happens in a vertical-coupling setup due to the increased length of the interaction region.

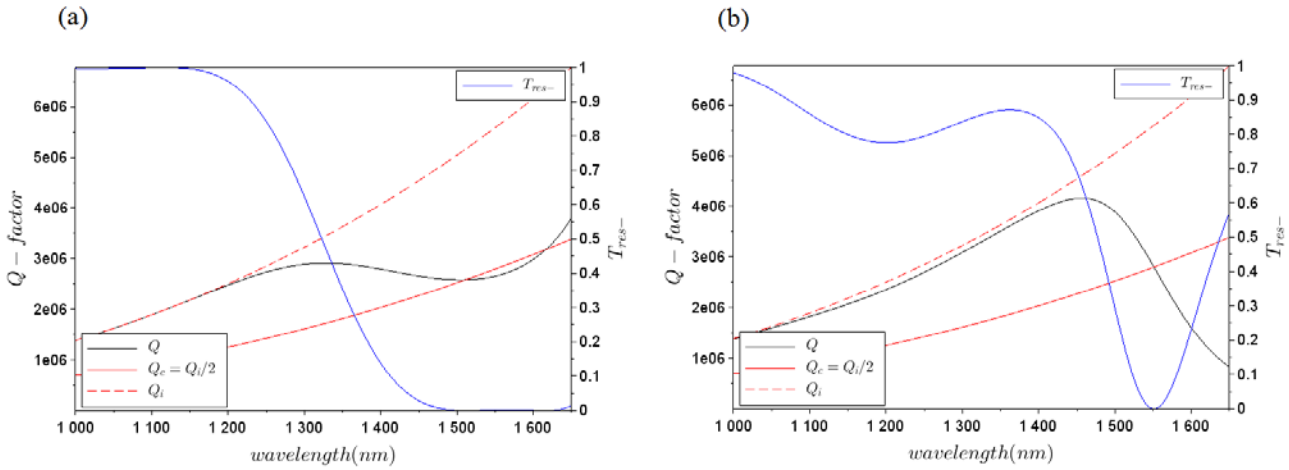

Figure 9. Representation of Q-factor and T_{res-} as a function of wavelength for (a) the second critical coupling length at 1550 nm. (b) the fifth critical coupling length at 1550 nm

6. CONCLUSIONS

We applied coupled-mode analysis to vertically-coupled micro-disk resonators presenting an asymmetric distribution of refractive index and a multilayer separation region between the two waveguide cores. In doing so, a criterion was introduced, which clarifies how to best choose the individual decomposition index profiles. We subsequently exploited the derived decomposition to evaluate the theoretical transmission characteristics of an AlGaAs/AlOx-based structure and showed that this latter is modulated by an envelop that governs the coupling regime of the resonator-waveguide system. It is then possible to optimize the tansmission bandwidth by adequately designing the structure of the coupler. Future work will focus on extending our analysis to phase-matched waveguides in order to explore other possibilites in the design of critically-coupled devices.

ACKNOWLEDGMENTS

Clément Arlotti would like to acknowledge the Délégation Générale de l'Armement and the Centre National d'Etudes Spatiales for supporting his PhD studentship. The work was also partly supported by the Centre National d'Etudes Spatiales research Grant R et T: R-S13-LN-0001-025 and the French Renatech Network of cleanroom facilities.

REFERENCES

[1] Matsko, A. B., Ilchenko, V. S., "Optical resonators with whispering gallery modes I: basics," *IEEE J Sel Top Quantum Electron 12(1),* pp. 3–14, (2006).

[2] Ward, J., Benson, O, "WGM microresonators: sensing, lasing and fundamental optics with microspheres," *Laser Photonics Rev. 5(4)*, pp. 553–570, (2011).

[3] Feng, S., Lei, T., Chen, H., Cai, H., Luo, X.., Poon, A. W, "Silicon photonics: from a microresonator perspective," *Laser Photonics Rev. 6(2)*, pp. 145–177, (2012).

[4] Yariv, A. "Universal relations for coupling of optical power between microresonators and dielectric waveguides," *Electron. Lett.*, vol. 36, no. 4, pp. 321–322, (2000).

[5] Stoffer, R., Hiremath, K. R., Hammer, M., Prkna, L. and Čtyroký, J., "Cylindrical integrated optical microresonators: Modeling by 3-D vectorial coupled mode theory," *Opt. Commun.*, vol. 256, no. 1–3, pp. 46–67, (Dec. 2005).

[6] Ghulinyan M., Ramiro-Manzano F., Prtljaga, N., Guider, R., Carusotto, I., PitantiA., Pucker, G., Pavesi, L., "Oscillatory Vertical Coupling between a Whispering-Gallery Resonator and a Bus Waveguide," *Phys. Rev. Lett.*, vol. 110, no. 16, (Apr. 2013).

[7] Mandorlo F., Rojo Romeo, P., Letartre, X., Orobtchouk, R., and Viktorovitch, P. "Compact modulated and tunable microdisk laser using vertical coupling and a feedback loop," *Opt. Express*, vol. 18, no. 19, p. 19612, (Sep. 2010).

[8] Hardy, A. and Streifer, W., "Coupled mode theory of parallel waveguides," *J. Light. Technol.*, vol. 3, no. 5, pp. 1135–1146, (1985).

[9] Haus, H., Huang, P., Kawakami, S., and Whitaker, N., "Coupled-mode theory of optical waveguides," *J. Light. Technol.*, vol. 5, no. 1, pp. 16–23, (1987).

[10] Little, B. E., and. Huang, W. P., "Coupled-mode theory for optical waveguides.," *Progress In Electromagnetics Research 10*, pp. 217–270, (1995).

[11] Calvez, S., Lafleur, G., Larrue, A., Calmon, P.F., Arnoult, A., Almuneau, G., Gauthier-Lafaye, O., "Vertically Coupled Microdisk Resonators Using AlGaAs/AlOx Technology," *IEEE Photonics Technol. Lett.*, vol. 27, no. 9, pp. 982–985, (May 2015).

[12] Okamoto, K., [*Fundamentals of optical waveguides*]. San Diego: Academic Press, (2000).

[13] Borselli, M., Johnson, T.J., and Painter, O.,"Beyond the Rayleigh scattering limit in high-Q silicon microdisks: theory and experiment," *Opt. Express*, vol. 13, no. 5, p. 1515, (2005).